

An Experimental and Modeling Study of Shock tube and Rapid Compression Machine Ignition of *n*-Butylbenzene/Air Mixtures

Hisashi Nakamura^{1,2}, Daniel Darcy¹, Marco Mehl³, Colin J. Tobin¹, Wayne K. Metcalfe¹,
William J. Pitz³, Charles K. Westbrook³, Henry J. Curran¹

¹Combustion Chemistry Centre, National University of Ireland, Galway, Ireland

²Institute of Fluid Science, Tohoku University, 2-1-1 Katahira,

Aoba-ku, Sendai 980-8577, Japan

³Lawrence Livermore National Laboratory, CA 94551, USA

Corresponding author

Assistant Professor, Hisashi Nakamura

Institute of Fluid Science, Tohoku University,

2-1-1 Katahira, Aoba-ku, Sendai 980-8577, Japan

TEL: +81-22-217-5296

FAX: +81-22-217-5296

E-mail: nakamura@edyn.ifs.tohoku.ac.jp

Abstract

In our previous work (D. Darcy, C. J. Tobin, K. Yasunaga, J. M. Simmie, J. Würmel, W. K. Metcalfe, T. Niass, S. S. Ahmed, C. K. Westbrook, H. J. Curran, *Combust. Flame* 159 (2012) 2219–2232), ignition delay times of *n*-butylbenzene in air were measured using a shock tube over a temperature range of 980–1360 K, at reflected shock pressures of 1, 10, and 30 atm, and at equivalence ratios of 0.3, 0.5, 1.0 and 2.0. In the present study, these measurements have been extended to 50 atm and to lower temperatures using a rapid compression machine in the temperature range 730–1020 K, at compressed gas pressures of 10, 30 and 50 atm, over the same equivalence ratio range. Trends in ignition delay times over the wide temperature range were identified. The chemical kinetic model for *n*-butylbenzene, which was validated for the original shock tube data, was extended by adding low-temperature kinetics. The updated chemical kinetic model captures the general trend in reactivity of *n*-butylbenzene over the wide range of temperature, pressure and equivalence ratio conditions studied. Reaction flux analyses were carried out and it was found that fuel H-atom abstraction reactions forming the 4-phenylbut-4-yl radical, and its subsequent addition to molecular oxygen, is the primary source of reactivity in the low-temperature regime. High sensitivity to ignition delay time of the isomerization reactions of alkylperoxy, $\text{RO}_2 \rightleftharpoons \text{QOOH}$, and peroxy-alkylhydroperoxide radicals, $\text{O}_2\text{QOOH} \rightleftharpoons \text{carbonylhydroperoxide} + \dot{\text{O}}\text{H}$, was also observed at low-temperatures. Comparisons are also made with experimental data obtained for *n*-propylbenzene over the same range of conditions and common trends are highlighted. It was found that, in general, *n*-butylbenzene was faster to ignite over the lower temperature range of 650–1000 K.

Keywords

Ignition delay times; *n*-butylbenzene; oxidation; shock tube; rapid compression machine;

1. Introduction

Alkylbenzenes are one of the major components in diesel fuels [1] and fundamental knowledge of the chemical kinetics of alkylbenzene fuels is required for further improvement of diesel engines. Carbon numbers for alkylbenzenes in U.S. market diesels for diesel components range in size from approximately C9 to C20 [2][3]. Mueller et al. chose *n*-butylbenzene to be the representative species for alkyl-aromatics in eight components surrogate mixtures targeting two different diesel fuels [3]. Although diesel fuels contain alkylbenzenes with larger side-chains than *n*-butylbenzene, a study of alkylbenzenes with smaller side-chains, like *n*-butylbenzene, is a necessary first step to develop a fundamental understanding that can be used to develop chemical kinetic mechanisms of larger alkylbenzenes.

There has been extensive previous work on alkylbenzenes. Starting with the small alkylbenzenes, measurements and modeling studies have been performed for ignition delay times for toluene [4]–[12], ethylbenzene [9]–[14], xylenes [9][12][14]–[17] and *n*-propylbenzene [9][10][18]–[20] at various temperatures and pressures. In the case of *n*-butyl benzene, ignition characteristics as well as flame characteristics have been studied. In early work, Roubaud et al. measured ignition delay times of *n*-butylbenzene using a rapid compression machine in the low-temperature region (600–900 K), at compressed pressures of up to 20 bar, for stoichiometric mixtures of $[O_2]/[inert] = 0.27$ (air) [9] and 0.37 [15], and compared the reactivity of *n*-butylbenzene to similar xylenes. Modeling of the observed low-temperature oxidation of *n*-butylbenzene was conducted by considering an *n*-butane mechanism and taking into account the change of reactivity due to the introduction of the aromatic ring [21].

In our previous work on *n*-butylbenzene, Husson et al. [22] obtained experimental results for its oxidation using three different methods: ignition delay time measurements in a rapid

compression machine over a temperature range of 640–960 K, at compressed pressures from 13 to 23 bar, and at equivalence ratios of 0.3 to 0.5; ignition delay time measurements using a shock tube over a temperature range of 980–1740 K, at reflected shock pressures of 1, 10, and 30 atm, for equivalence ratios of 0.3, 0.5, 1.0 and 2.0; species concentration measurements in a jet-stirred reactor over a temperature range of 550–1100 K, at atmospheric pressure, and at equivalence ratios of 0.25, 1.0, and 2.0. They found a large role of the addition to molecular oxygen of resonantly stabilized, 4-phenylbut-4-yl radicals.

n-Butylbenzene has been investigated in other fundamental experimental devices. Diévert and Dagaut [23] studied the diluted oxidation of *n*-butylbenzene using a jet-stirred reactor over the temperature range 550–1150 K at 10 atm for equivalence ratios from 0.25 to 1.5. Won et al. [24] and Ji et al. [25] studied *n*-butylbenzene extinction limits of counter-flow diffusion flames at atmospheric pressure. Ji et al. also reported laminar flame speeds of *n*-butylbenzene/air mixtures at equivalence ratios from 0.7 to 1.5 and at atmospheric pressure. Pousse et al. [26] studied the high temperature behavior of methane/*n*-butylbenzene/O₂/Ar mixtures by measuring temperature and species concentration profiles in a low pressure flat flame at 6.7 kPa, at an equivalence ratio of 0.74, with a ratio of methane/*n*-butylbenzene of 13.5%, and with an oxygen mole fraction of 36.8%. In these studies [24] and [25], kinetic models of *n*-butylbenzene were extensively validated using the experimental results. However, the temperature, pressure and equivalence ratio conditions of these experiments do not fully cover those experienced in diesel engines, especially at low-temperature, high-pressure, and high equivalence ratio conditions. Experimental results over a wider range of conditions are necessary to develop and validate a chemical reaction mechanism for diesel engines as well as obtaining a fundamental knowledge of the chemical kinetics under these relevant conditions.

The objective of this study is to measure and predict ignition delay times for *n*-butylbenzene/air mixtures over a wide range of temperatures, pressures, and equivalence

ratios. Using both a rapid compression machine and a shock tube, the experimental conditions ranged over temperatures of 730–1360 K, pressures of 10, 30, 50 atm, and equivalence ratios of 0.3, 0.5, 1.0 and 2.0. Our previous mechanism which described only high-temperature chemistry has been updated to include the low-temperature reactions in which the fuel radicals add to molecular oxygen and proceed to chain branching through a series of isomerization reactions. Measured ignition delay times have been compared with the model predictions and the detailed oxidation of *n*-butylbenzene is described.

2. Experimental

2.1 Rapid compression machine

Ignition delay times at low temperature were measured using an opposed-piston rapid compression machine originally developed by Affleck and Thomas at Shell-Thornton [27] and re-commissioned at NUIG in the late 1990s [28][29]. Creviced piston heads, with an inner diameter of 38.2 mm, were used in order to improve the post-compression temperature homogeneity in the combustion chamber [30]. The compression ratio was approximately 13:1 in this study. Experimental compression times are relatively short at approximately 16 ms compared to > 20 ms in single piston RCM facilities [31][32]. In order to attain the desired pressure and temperature at the end of compression, the initial pressures and temperatures and inert gas compositions (N₂, Ar and CO₂) were varied. A silicone-coated pressure transducer (Kistler; 603B) was installed in the combustion chamber and pressure traces were recorded using a digital oscilloscope (Pico Technology; PicoScope 4244 PC Oscilloscope). The compressed gas temperature was calculated using Gaseq [33]. Figure 1 shows a typical pressure trace obtained from the NUIG rapid compression machine. The ignition delay time was defined as the time interval between the time of maximum pressure near the end of compression and the maximum rate of rise of the pressure signal due to ignition. Non-reactive experiments were performed in which oxygen was replaced by nitrogen in a mixture, in order

to obtain pressure-time histories which are converted to volume-time histories to be used in chemical kinetic simulations to simulate the effects of compression and heat loss. Details of the facility and experimental procedures are given in [34][35].

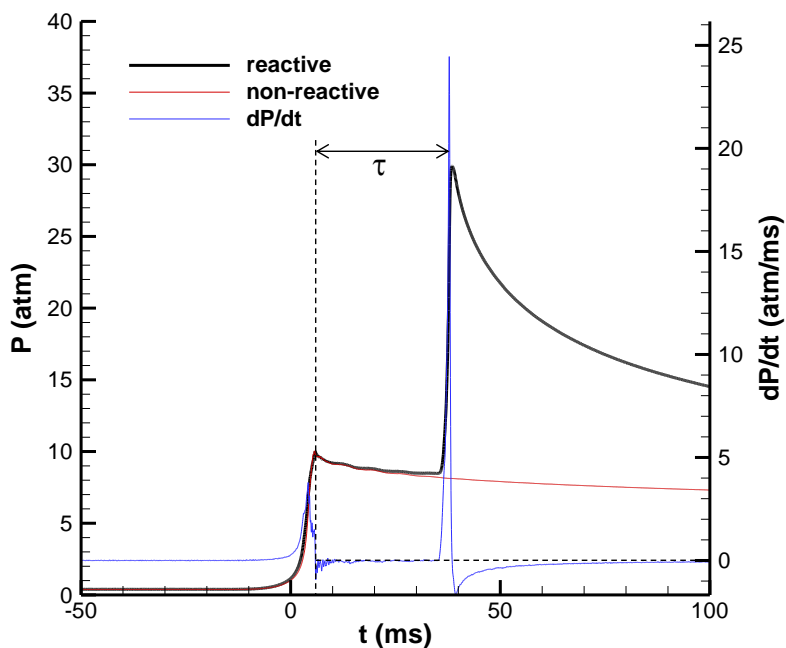


Figure 1: Typical pressure trace obtained from the NUIG rapid compression machine; $\phi = 1.0$, compressed gas pressure = 10 atm, compressed gas temperature = 893 K.

The RCM heating system was updated to ensure no condensation of *n*-butylbenzene, which has a saturation vapor pressure of 0.13 kPa at 298 K [36]. A double-stranded heating tape (Flexelec, 250 W) was wrapped around the surface of the combustion chamber and two double-stranded heating tapes (Flexelec, 250 W) were wrapped along the length of the two sleeve sections of the RCM. Insulation (Zetex 1000) was wrapped over the heating tape. Six cartridge heaters (hotrod® Type HHP 6.5 mm) were inserted into the sleeve wall around the piston head at the start of the compression. In total, twelve cartridge heaters were used for both sleeves. The heating tapes and the set of the six cartridge heaters were connected to five thermostats (CAL Controls; CAL 9900). Ten thermocouples were placed on the surface of the sleeves and of the combustion chamber. Five thermocouples were connected to the

thermostats to control the temperature while the others were used to monitor the temperature to ensure homogeneity. Figure 2 shows some examples of temperature profiles inside the sleeve. Typically, a temperature drop may be observed near the piston head since heat loss through the piston head and through the rod can be significant. However, the present heating system worked well and we did not observe an appreciable temperature drop near the piston head. The variation of the temperature profiles is approximately ± 1.0 K.

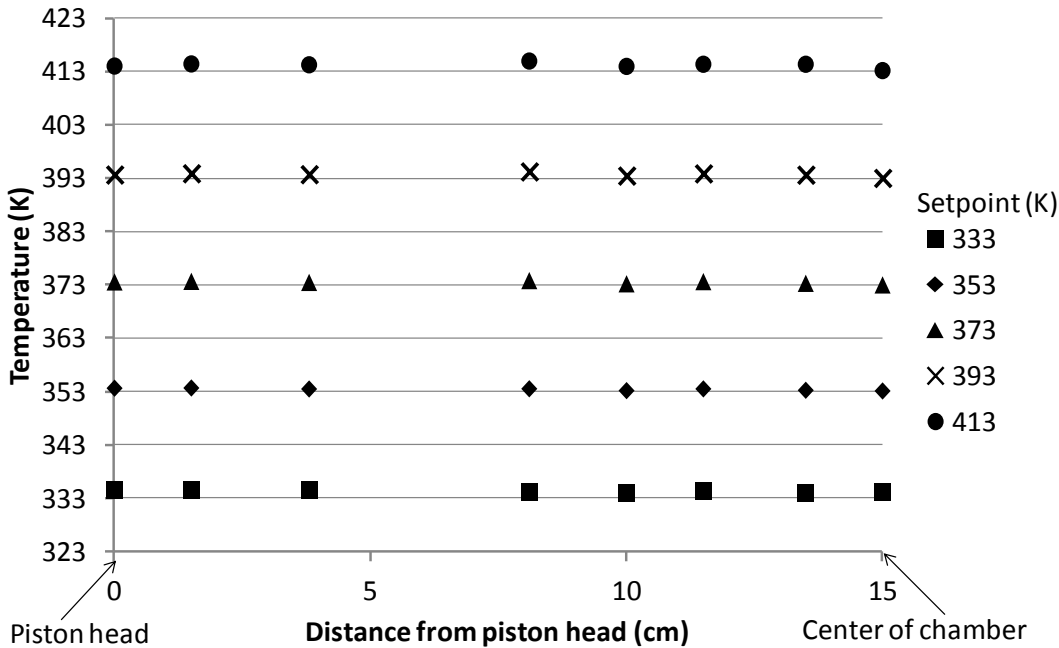


Figure 2: Temperature profiles inside RCM sleeve and chamber.

The heating system was extended to the manifold and to the two mixing tanks where several double-stranded heating tapes (Flexelec, 1250 W) and insulation (Zetex 1000) were used. Two thermostats (CAL Controls; CAL 9900) were used for the manifold and one mixing tank and, overall, six thermostats were used for the manifold and for the two mixing tanks. Twelve thermocouples were placed on the surface of the manifold and the mixing tanks. Six thermocouples were connected to the thermostats to control the temperature and the others were used to monitor the temperature to ensure homogeneity and that no cold spots occurred.

All mixtures were left for at least one hour before use in both the RCM and in the shock tube to ensure homogeneous charge composition. Mixture compositions were verified by in-situ testing using an infra-red laser system described in detail in [37] similar to that used by Mével et al. [38] who studied gas phase absorption cross sections at 3.39 μm to determine the concentration of twenty-one liquid hydrocarbons in the temperature range 303–413 K using an infrared He–Ne laser. Figure 3 shows the evolution of $-(1/L)\cdot\ln(I/I_0)$ as a function of the fuel concentration for *n*-butylbenzene. Using this correlation, we were able to verify that no *n*-butylbenzene condensation occurred in our RCM experiments and the *n*-butylbenzene concentration measured in the shock tube was same as the concentration computed from its partial pressure in the mixing tank.

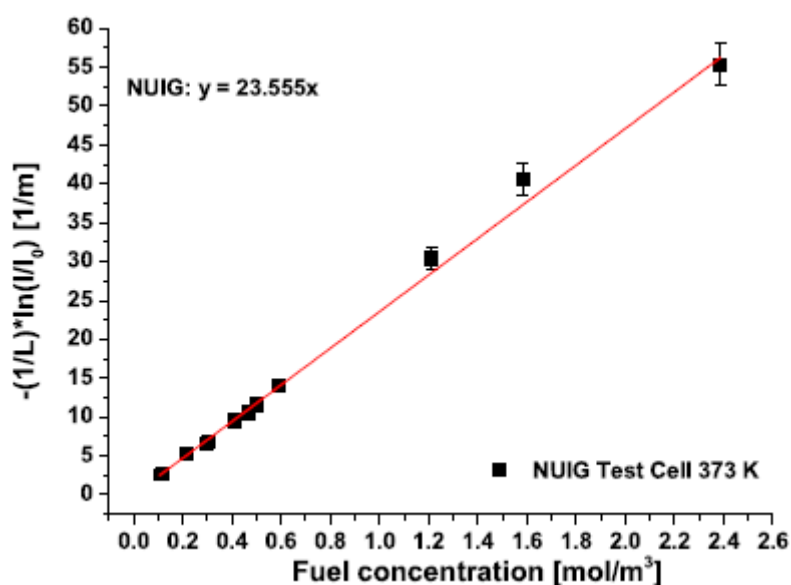


Figure 3: Evolution of $-(1/L)\cdot\ln(I/I_0)$ as a function of *n*-butylbenzene fuel concentration at 338.15 K.

The RCM experiments were conducted at compressed pressures of 10, 30 and 50 atm for equivalence ratios of 0.3, 0.5, 1.0 and 2.0. However, due to the very low vapor pressure of the fuel (1.03 mm Hg at 20°C), experiments at a compressed pressure of 50 atm and at an

equivalence ratio of 2.0 were not possible. This gave a total of 11 different experimental data sets. Estimated uncertainty limits of the measurements are ± 5 K in compressed gas temperature, $\pm 5\%$ in compressed gas pressure, and $\pm 10\%$ in ignition delay time.

2.2 Shock tube

Ignition delay times were measured at high temperature using a high-pressure shock tube. The previous shock tube [20] was replaced so that we could perform higher pressure experiments with the operational pressure limit of the present shock tube being approximately 100 atm. Ignition delay times of *n*-butylbenzene/air mixtures at 50 atm were newly obtained and those at lower pressure were published previously [22]. The size of the present shock tube is the same as that of the previous one (9.0 m in length; 63.5 mm in the internal diameter). A double-diaphragm section divides the tube into a 3 m long driver section and a 5.7 m driven section. Aluminum plates were used as the diaphragm material, where the thickness of the diaphragms was chosen depending on the desired final shock pressure and varied from 0.8–2.0 mm. A helium (99.99% pure; BOC) and nitrogen (99.99% pure; BOC) mixture were used as the driver gas, where the mixing ratio was chosen depending on the desired final shock pressure and test duration and varied from 75:25 to 100:0 (He:N₂). Six pressure transducers on the sidewall (PCB; 113A24) and one at the endwall (Kistler; 603B) were used to measure the velocity of the incident shock wave, which was used to calculate the temperature of the mixtures behind the reflected shock wave using the program Gaseq [33]. The uncertainty of temperature behind the reflected shock wave was estimated to be ± 15 K. Pressures behind the reflective shock wave were measured using the pressure transducer in the endwall. Pressure traces were obtained using two digital oscilloscopes (TiePie Handyscope HS4 oscilloscope). The ignition delay time was defined as the interval between the rise in pressure due to the arrival of the incident shock wave at the endwall and the maximum rate of rise of the pressure signal. The pressure rise before ignition is approximately

3 %/ms in the present shock tube.

A heating system was designed and installed on the driven section and manifold of the shock tube to ensure that no condensation of *n*-butylbenzene occurred. Double-stranded heating tapes (Flexelec, 1250 W) were wrapped along the length of the driven section and along part of the driver section with thermocouples positioned at regular intervals. The heating tapes and thermocouples were connected to thermostats (DigiTrace ICON 4848). Rock wool insulation was wrapped over the heating tape and covered with an insulating blanket to ensure minimal heat loss to the atmosphere. This heating system maintained temperatures within ± 1.0 K.

The heating system was extended to the manifold where three rope heaters (Omega, FGR) and one single-stranded heating tape (Flexelec, 1250 W) were wrapped directly onto the surface of the manifold. The ropes and heating tape were attached to four separate thermostats (Vulcanic 30633, 2 amp output), controlled by thermocouples. The sensors measured the temperature at different locations to ensure homogeneity and no cold spots. The heating ropes and tape on the manifold were finally wrapped with insulation tape (Zetex 1000). The heating system design used on the driven section of the shock tube was repeated to heat the two mixing tanks used herein, with three thermostats (Flexelec, 16 amp) used per tank. Estimated uncertainty limits of the measurements are $\pm 1\%$ in reflected shock temperature, T_5 , and $\pm 15\%$ in ignition delay time, τ .

2.3 Mixture preparation

Table 1 shows the composition of the mixtures prepared in this study. The volumetric ratio of oxygen to diluent is the same as that of air and this means that O_2 concentration in the reactant mixture changes little for the four different equivalence ratio mixtures considered. *n*-Butylbenzene was obtained from Tokyo Chemicals Ltd at 99% purity (GC grade) and oxygen (99.5%) was supplied by BOC Ireland. Nitrogen (99.99%) supplied by BOC Ireland

was used as the diluent in the shock tube experiments. Mixtures of nitrogen (99.99%), argon (99.99%) and carbon dioxide (99.99%) were used as the diluent in the RCM experiments.

Table 1 Composition of mixtures.

ϕ	% fuel	% O ₂	% diluent
0.3	0.46	20.90	78.64
0.5	0.77	20.84	78.39
1.0	1.53	20.68	77.79
2.0	3.02	20.37	76.61

Mixtures were prepared in the heated mixing tanks. The fuel was injected via an injection port on the tank using a gas-tight syringe (SGE Analytical Science, 5ml volume, 008760). To ensure no fuel condensation in the tank, the fuel partial pressure was maintained at a value less than one third that of the fuel vapor saturation pressure at the given temperature. The amount of the fuel injected was controlled by measuring the tank pressure using an MKS pressure transducer and also by using the difference of weights of the syringe before/after the injection using an electric balance. Thereafter, oxygen and diluent were added to the tank to the desired pressure. The uncertainty of mixture concentration was estimated to be $\pm 2\%$.

3. Chemical kinetic modeling

A revised chemical kinetic model for *n*-butylbenzene has been developed. The molecular structure of *n*-butylbenzene is given in Fig. 4 with the various radical sites on the *n*-butyl side-chain labeled for use in this section and later in the paper.

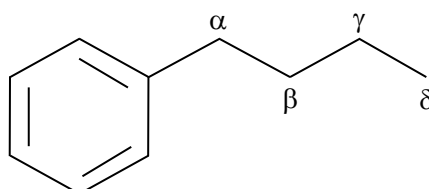


Figure 4: Molecular structure of *n*-butylbenzene and labels of *n*-butyl side-chain.

The present chemical kinetic model was initially derived by merging the recently published

C₀–C₄ kinetic mechanism developed at Galway (AramcoMech 1.3) [39] with the toluene mechanism by Metcalfe et al. [40] and the alkyl-aromatics sub-mechanism published previously by Darcy et al. [41]. This mechanism has been extended to include more detailed cyclopentadiene chemistry, including the addition and recombination reactions of C₅H₅ radicals to form larger aromatic species. These modifications included the adoption of reaction rates derived from the theoretical study performed by Cavallotti et al. [42] and were verified through the validation against flow reactor data by Butler and Glassman [43]. A more extensive description of heavier aromatic species, such as indene and naphthalene has also been introduced, including the reactions leading to the formation and the subsequent oxidation of naphthalene and indene. The sub-mechanism for these polycyclic aromatic species has been derived from the Narayanaswamy et al. mechanism [12]. A more detailed discussion on the changes introduced in the toluene submechanism can be found in [44].

The alkyl aromatic mechanism (including ethylbenzene, *n*-propylbenzene and *n*-butylbenzene) is based on the mechanism proposed by Diévarit and Dagaut [23]. In our prior work [41], the *n*-propylbenzene portion of the model was updated by revising the reaction rate constants for the hydrogen abstractions on the alkyl chain of the fuel. These changes have been extended to the butyl benzene portion of the mechanism adopting the same reaction rules of [41]. Similarly, the secondary benzyl radical + HO₂ reaction leading to the formation of the benzoxy and radicals has been set to $1 \times 10^{13} \text{ cm}^3 \text{ mol}^{-1} \text{ s}^{-1}$, as proposed in [40] for the primary benzyl radical of toluene. Beta-decomposition reactions of the phenyl-butyl radicals were specified in the exothermic direction.

The existing low temperature mechanism for *n*-butylbenzene has been modified using the low temperature mechanism of 1-hexene as a model. Both fuels, 1-hexene and butylbenzene, have a 4 carbon saturated chain where the first secondary carbon site can generate a resonantly stabilized radical. For this reason, the reaction rates for the low temperature

branching paths active on the alkyl chain of the fuel molecules were directly derived from the alkene mechanism by Mehl et al. [45], assuming that the allylic site in the olefin chain corresponds to the benzylic one present in the aromatic structures. The use of a set of reaction rates derived from a consistent body of reaction rules developed over the years by the NUI/LLNL combustion group allowed for the compilation of an integrated and systematic approach to the modeling of alkyl aromatics, resulting in more reliable predictions of the branching ratios of different fuels belonging to this class of compounds.

As described in our recent *n*-propylbenzene paper [44], the addition reactions of the benzyl radical to molecular oxygen, an important step in the low temperature mechanisms of alkylbenzenes in general, have been derived by fitting over the temperature range of interest (600–900 K) the reaction rates that have been theoretically calculated by Murakami et al. [46] for the xylyl + O₂ system. The reaction rate for the concerted elimination of HO₂ radical from the alkylperoxy species have been derived from Altarawneh et al. [47], as in [44].

The thermodynamic properties for the low temperature species involved in the *n*-butylbenzene mechanism were estimated using the THERM program developed by Ritter and Bozzelli, implementing Benson's group additivity method [48, 49]. These new estimations corrected significant errors in the thermodynamic parameters for the low temperature *n*-butylbenzene species compared to the previous model. Also, critical R–O₂ bond energies were updated with the new THERM estimates. For the alpha radical (4-phenylbut-4-yl radical)–O₂ (secondary benzylic), the new value resulting from the updated THERM calculations is now 23.7 kcal mol⁻¹, a value reasonably close to the 24.6 kcal mol⁻¹ proposed by [47]. This bond energy is significantly higher than for benzyl–O₂ (primary benzylic) of 19.7 kcal mol⁻¹ based on the thermodynamic properties we are using for benzyl [40] and RO₂ radicals from THERM. It is worth stressing how these values are significantly lower than the R–O₂ bond strength calculated for non-resonantly stabilized secondary alkyl

radicals (38 kcal mol^{-1}). The correct evaluation of the relative bond energies in the $\dot{\text{R}}\text{-O}_2$ for alkyl aromatic systems (secondary benzylic $\dot{\text{R}}\text{-O}_2$ compared to the primary benzylic, compared to the secondary alkyl) is an important factor in reproducing the experimental behavior observed in the NTC region and in showing the significance of the addition of the alpha radical (4-phenylbut-4-yl radical) to molecular oxygen and subsequent low temperature branching reactions. This important point will be explained in more depth in the discussion section. The resulting mechanism includes about 960 species and 4330 and is included along with thermodynamic properties in the Supplemental Material of our recent *n*-propylbenzene paper [44].

The CHEMKIN-Pro (version 15101) transient closed homogeneous batch reactor was used to validate the model against shock tube and RCM data. For the simulations of RCM experiments, variable volume-time histories were employed to include facility effects including reaction during compression and heat loss. These variable volume-time histories were generated from non-reactive pressure traces. All non-reactive pressure traces are available as Supplemental material. For shock tube simulations, constant volume conditions were employed and no facility effects were included because ignition delay times measured by the present shock tube are shorter than 2 ms in most cases and the present pressure rise before ignition due to the facility effects (3 %/ms) does not significantly affect the simulation of such short ignition delay times. (Ex. 2.0 ms without the pressure rise vs. 1.7 ms with pressure rise, 1.0 ms without the pressure rise vs. 0.92 with the pressure rise)

4. Results and discussion

4.1 Effect of pressure on ignition delay time

Figure 5 shows the effect of pressure on ignition delay times for equivalence ratios of 0.3, 0.5, 1.0 and 2.0 from the experiments and computations. From the experimental results, ignition delay times decrease with increasing pressure at all equivalence ratios. The pressure

dependence of ignition delay times in the shock tube regime at an equivalence ratio of 0.3 is less than that at the other equivalence ratios. Focusing first on the equivalence ratio of 0.3 (Fig. 5a), ignition delay times at all pressures exponentially increase with an increase in inverse temperature. However, for the 50 atm curve in the low-temperature regime, (at approximately $10^4 \text{ K} / T > 11.5$, $T < 870 \text{ K}$) the slope of the curve decreases significantly. Similar trends can be seen at the equivalence ratio increases to 0.5 (Fig. 5b) and 1.0 (Fig. 5c). The increase of ignition delay time with an increase in inverse temperature is very small or nearly constant in the low-temperature regime at 30 and 50 atm. At an equivalence ratio of 2.0 (Fig. 5d), the decrease of ignition delay time with an increase of inverse temperature, so-called negative temperature coefficient (NTC) behavior, can be seen in the low temperature region at 10 and 30 atm. The present chemical kinetic model accurately predicts experimental ignition delay times although there are discrepancies between the experiments and predictions at very low temperatures (approximately at $10^4 \text{ K} / T > 12.5$).

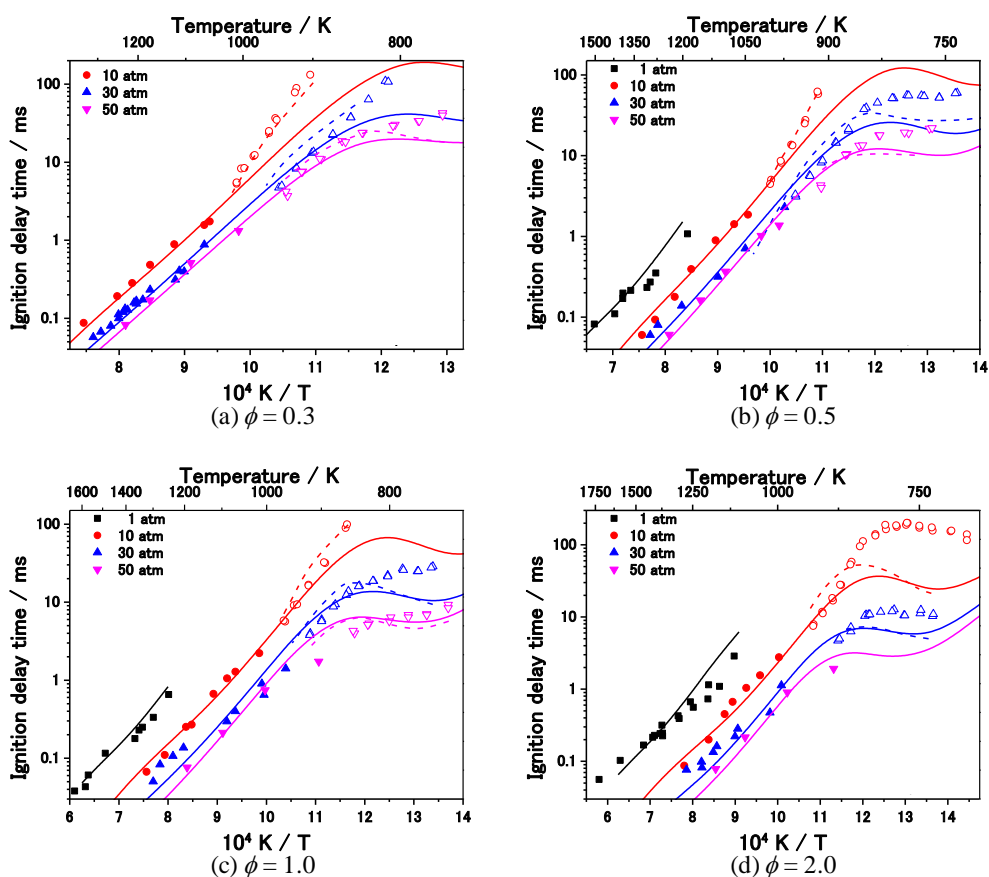


Figure 5: Effect of pressure on ignition delay time; ■: 1 atm; ●: 10 atm; ▲: 30 atm; ▼: 50 atm; Solid symbols: shock tube; Open symbols: RCM; Solid line: Adiabatic simulation; Dashed line: RCM simulation including facility effects.

NTC behavior was observed only at high-pressure and high equivalence ratio conditions. However, the decrease of ignition delay time with an increase of inverse temperature is not as large and clear as in *n*-alkanes. It is interesting to compare the present results to *n*-butane whose size is similar to the alkyl chain is similar in size to the alkyl chain on *n*-butylbenzene. *n*-Butane/“air” mixtures [50] have shown more clear NTC behavior over a wide range of pressure and temperature compared to *n*-butylbenzene/“air” mixtures. Since the bond strength for $\dot{R}-O_2$ is less for *n*-butylbenzene ($23.7 \text{ kcal mol}^{-1}$) on the alpha (benzylic site), Fig. 4, than on a secondary site on an *n*-alkane ($\approx 38 \text{ kcal mol}^{-1}$), the $R\dot{O}_2$ species for *n*-butylbenzene tends to decompose to $\dot{R} + O_2$ and not then undergo low temperature pathways (discussed

later) that lead to chain branching as readily as *n*-butane. As a result, NTC behavior for *n*-butylbenzene is seen only at high-pressure and higher fuel/air equivalence ratio (≥ 1.0) conditions that are very favorable for low temperature chemistry.

Figure 6 shows a comparison between the present experimental results and the prediction of ignition delay times using the previous chemical kinetic model published by Husson et al. [22]. In the shock tube, the previous model predicts well the experimental ignition delay times at 1 and 10 atm within a factor of 1.5 and 2 respectively for all of the equivalence ratios. By comparison, the current model has slightly better agreement at 1 atm and much better agreement at 10 atm. At 30 and 50 atm, simulated ignition times using the Husson et al. [22] model are 2–3 times longer than those measured in the experiments. Overall, the Husson model does not reproduce well the effect of pressure in the shock tube over the range of 1 to 50 atm, while the present model reproduces the pressure effect. Reproducing the effect of pressure is critical for modeling ignition in internal combustion engines. In the RCM regime at all pressures and equivalence ratios, the simulated ignition times of the Husson et al. [22] model are 2–4 times longer than those measured in the experiments, except at an equivalence ratio of 2.0 at very low temperatures (approximately $10^4 / T > 12.5$, $T < 800$ K). These discrepancies are not as pronounced in the comparison between experiments and computations using the present chemical kinetic model (Fig. 5), where the current model has significantly improved predictions of ignition delay times.

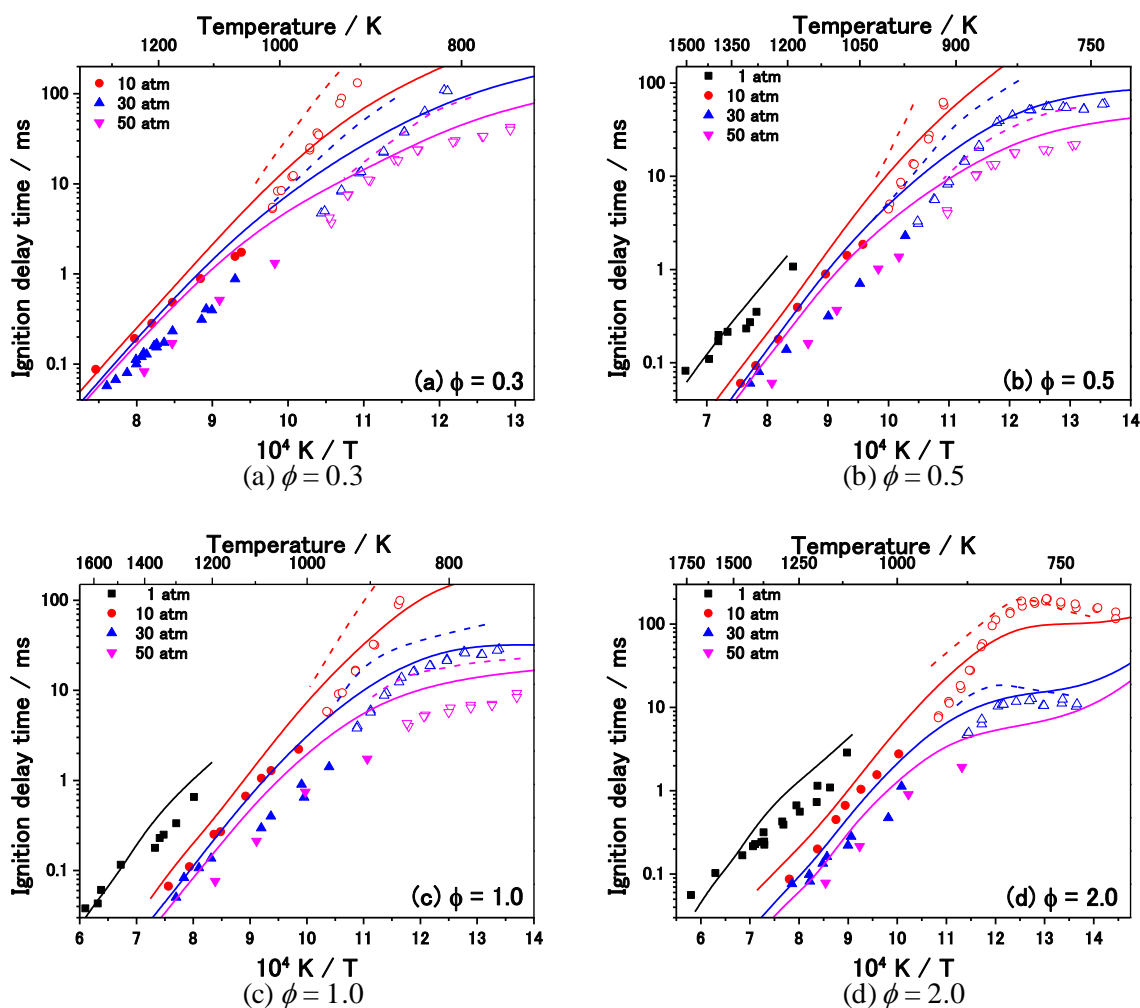


Figure 6: Effect of pressure on ignition delay time; previous chemical kinetic model [22] was used for simulation; ■: 1 atm; ●: 10 atm; ▲: 30 atm; ▼: 50 atm; Solid symbols: shock tube; Open symbols: RCM; Solid line: Adiabatic simulation; Dashed line: RCM simulation including facility effects.

The comparison between the main reaction pathways leading to the butylbenzene autoignition in the two models highlights how the two mechanisms are more similar than different. Analogous reaction pathways are responsible for the low temperature oxidation of the fuels even though the concerted elimination reactions included in the present mechanism are not included in the Husson et al. one, where the $\dot{R}+O_2=Olefin+HO_2$ oxidation reactions are adopted. Also, another important difference between the two models is the presence of

termination reactions in the Husson et al. mechanism leading to the formation of heavy alkyl-aromatic species that lack consumption pathways.

Preliminary tests however shown that these differences only account for a fraction of the deviation observed between the two models, and most likely dissimilarities in the C0–C4 mechanism and in the general reaction rules adopted to generate the model are responsible for the reduced reactivity of the Husson et al. mechanism compared to the current one.

4.2 Effect of equivalence ratio on ignition delay time

Figure 7 shows the effect on ignition delay times of varying the equivalence ratio for pressures of 10, 30 and 50 atm. This is the same ignition delay data presented in Fig. 5, but plotted to more easily see the effect of equivalence ratio. Experimental ignition delay times in the RCM decrease with an increase of equivalence ratio at all pressures. For the shock tube results, ignition delay times at 10 atm are almost insensitive to equivalence ratio. The equivalence ratio dependence of ignition delay times increases with an increase in pressure.

For the 10 atm experimental results in RCM (Fig. 7a), ignition delay times are linear for equivalence ratio of 0.3, 0.5 and 1.0 on a logarithmic scale as a function of inverse temperature. However, this linearity is only for an equivalence ratio of 0.3 at 30 atm (Fig. 7b) and no linearity is observed at 50 atm (Fig. 7c). The NTC behavior or the near-NTC behavior can be seen in the other conditions.

The chemical kinetic model follows the experimental behavior relatively well up to an inverse temperature of about 12 (corresponding to about 800 K). For temperatures below this, the computed ignition delay times in the RCM (represented by the dashed curves), are in general shorter than the experimentally measured times and more NTC behavior is seen in the model compared to the experiments. These are discrepancies in ignition delay corresponding to factors of about 1.5 to 9 for the 12 different cases. The following reaction flux and

sensitivity analysis will help to identify the reason for these differences and point to the areas where further work is needed to understand the low temperature chemistry of alkylbenzenes.

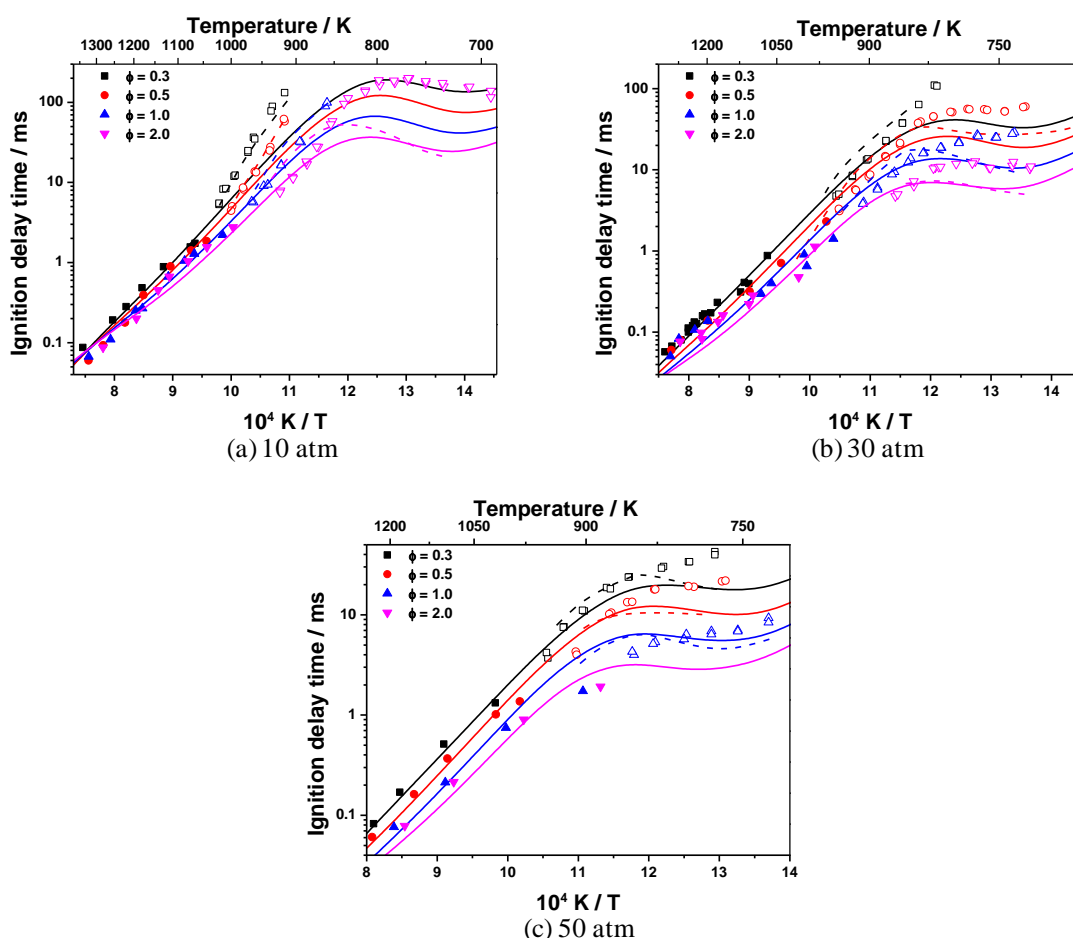


Figure 7: Effect of equivalence ratio on ignition delay time; ■: $\phi = 0.3$; ●: $\phi = 0.5$; ▲: $\phi = 1.0$; ▼: $\phi = 2.0$; Solid symbols: shock tube; Open symbols: RCM; Solid line: Adiabatic simulation; Dashed line: RCM simulation including facility effects.

4.4 Reaction flux analysis

A reaction flux analysis was carried out at $\phi = 1.0$, 30 atm and at 15% fuel conversion for a series of temperatures (750, 1000 and 1400 K) in order to investigate the important reactions controlling *n*-butylbenzene oxidation. The temperatures of 750, 1000 and 1400 K sample the temperature regions corresponding to low, intermediate and high temperature chemistry. The five major reaction pathways for *n*-butylbenzene are shown in Fig. 8. Black, red and blue numbers labeling the pathways represent percent consumption of *n*-butylbenzene at 1400,

1000 and 750 K, respectively.

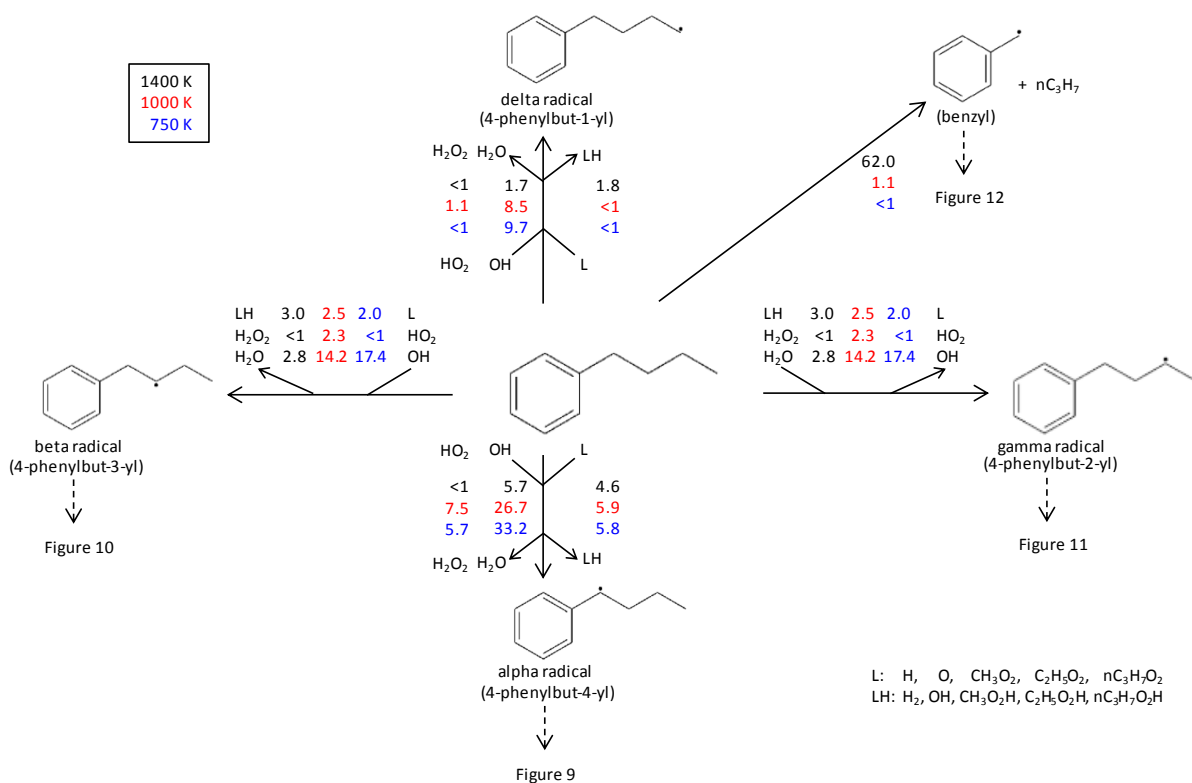


Figure 8: Primary reactions from *n*-butylbenzene and their fluxes at $\phi = 1.0$, 30 atm and 15 % fuel conversion. Numbers are percent contribution to the consumption of *n*-butylbenzene. “L” is the sum of contributions from the radical species listed.

At 750 K, the main consumption pathways for *n*-butylbenzene are H-atom abstraction reactions from the alkyl chain, mainly by $\dot{\text{O}}\text{H}$ radicals. Strong selectivity on the alpha- site (Fig. 4) is observed (33.2% with $\dot{\text{O}}\text{H}$, 44.7% for all radicals). Selectivity on the beta site (Fig. 4) is the same as that on the gamma site (17.4% with $\dot{\text{O}}\text{H}$, 20% with all radicals) since these sites use the same reaction rate rule. Selectivity on the delta- (primary) site shows the smallest flux among the H-atom abstraction reactions (9.7% with $\dot{\text{O}}\text{H}$, 11% with all radicals). At this low temperature, unimolecular fuel decomposition hardly proceeds. These trends are also observed at 1000 K. However, the importance of H-atom abstraction reactions by $\dot{\text{O}}\text{H}$ radical

at 1000 K is lower compared to that at 750 K (ex. 33.2% at 750 K and 26.7% at 1000 K for the alpha site) while the importance of H-atom abstraction reactions by HO_2 radical at 1000 K is slightly higher than that at 750 K (ex. 5.7% at 750 K and 7.5% at 1000 K for the alpha site). At 1400 K, unimolecular fuel decomposition is dominant and the H-atom abstraction reactions are far less important compared to the lower temperature conditions.

Figure 9 shows reaction pathways for the consumption of alpha (4-phenylbut-4-yl) radical. Since little alpha radical is formed at 1400 K, only fluxes at 750 and 1000 K are shown in the figure. At 750 K, the alpha radical mainly reacts with peroxy radicals and 4-phenylbut-4-oxidanyl radical is formed. This radical subsequently decomposes to benzaldehyde and an *n*-propyl radical. Benzaldehyde is one of the important intermediates experimentally observed at low temperature oxidation of *n*-butylbenzene below 800 K [22] and the mechanism employed in that study greatly underpredicted its concentration. A fraction of alpha radicals (13.7%) react with O_2 and 4-phenylbut-4-ylperoxy radicals are formed, which are mainly converted (50.8%) to phenyl radicals through a sequence of isomerization, O_2 addition, $\dot{\text{O}}\text{H}$ production and decomposition reactions. This is the path that is mainly responsible for low temperature chain branching through the production of $\dot{\text{O}}\text{H}$ radicals. A fraction of 4-phenylbut-4-ylperoxy radicals (17%) are also converted to 1-butenyl-benzene which reacts with $\dot{\text{O}}\text{H}$ radical and decomposes to benzaldehyde + *n*-propyl radicals and benzyl radicals + propanal. Propanal was also an important low temperature intermediate observed by Husson et al. [22] for *n*-butylbenzene oxidation. At 1000 K, on the other hand, alpha radicals mainly decompose to styrene and ethyl radicals, while its addition to O_2 hardly occurs.

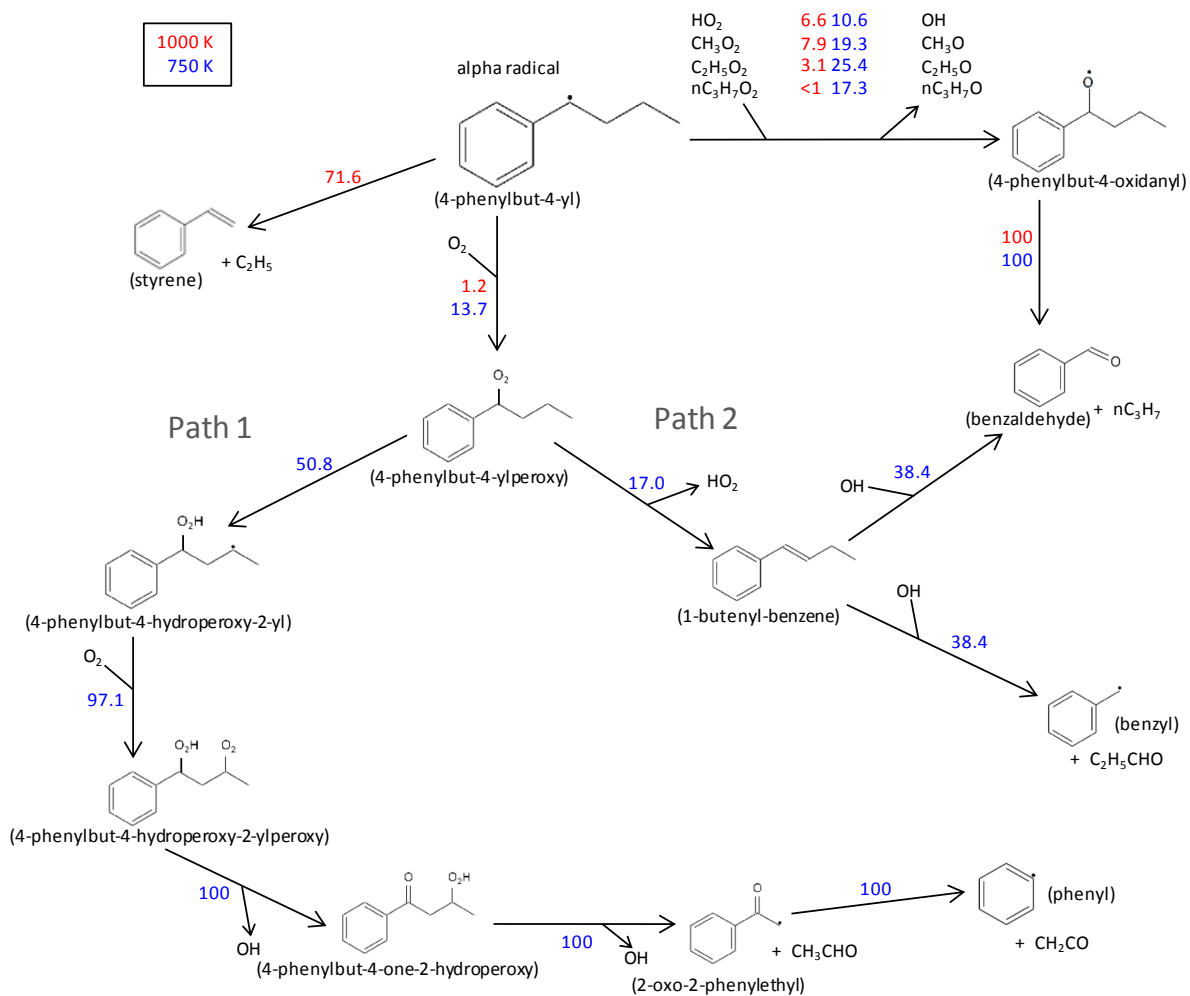


Figure 9: Reaction pathways following alpha (4-phenylbut-4-yl) radical at $\phi = 1.0$, 30 atm and 15 % fuel conversion. Numbers are percent contribution to the consumption of the species on the source side of the arrow.

Figure 10 shows reaction pathways consuming the beta (4-phenylbut-3-yl) radicals. At 750 K, beta radicals react with molecular oxygen and 4-phenylbut-3-ylperoxy radicals are formed. There are three major reaction channels from 4-phenylbut-3-ylperoxy radicals: 2-phenylethyl radical formation via 2-butenyl-benzene formation; 1-butenyl-benzene formation via HO₂ radical elimination; and 1-butenyl-benzene formation via isomerization. The 1-butenyl-benzene so produced reacts with OH radicals and decomposes to benzaldehyde + *n*-propyl radical and benzyl radical + propanal, as shown in Fig. 9. At 1000 K, nearly half of all beta radicals react with O₂ to generate 4-phenylbut-3-ylperoxy radicals. Reaction pathways

n-propylbenzene [44]; and benzenepropanal formation. The benzenepropanal is converted to 2-phenylethyl radical via H-atom abstraction by $\dot{\text{O}}\text{H}$ and $\text{H}\dot{\text{O}}_2$ radicals and via decomposition reactions. At 1000 K, 39.6% of gamma radicals decompose to a benzyl radical and propylene.

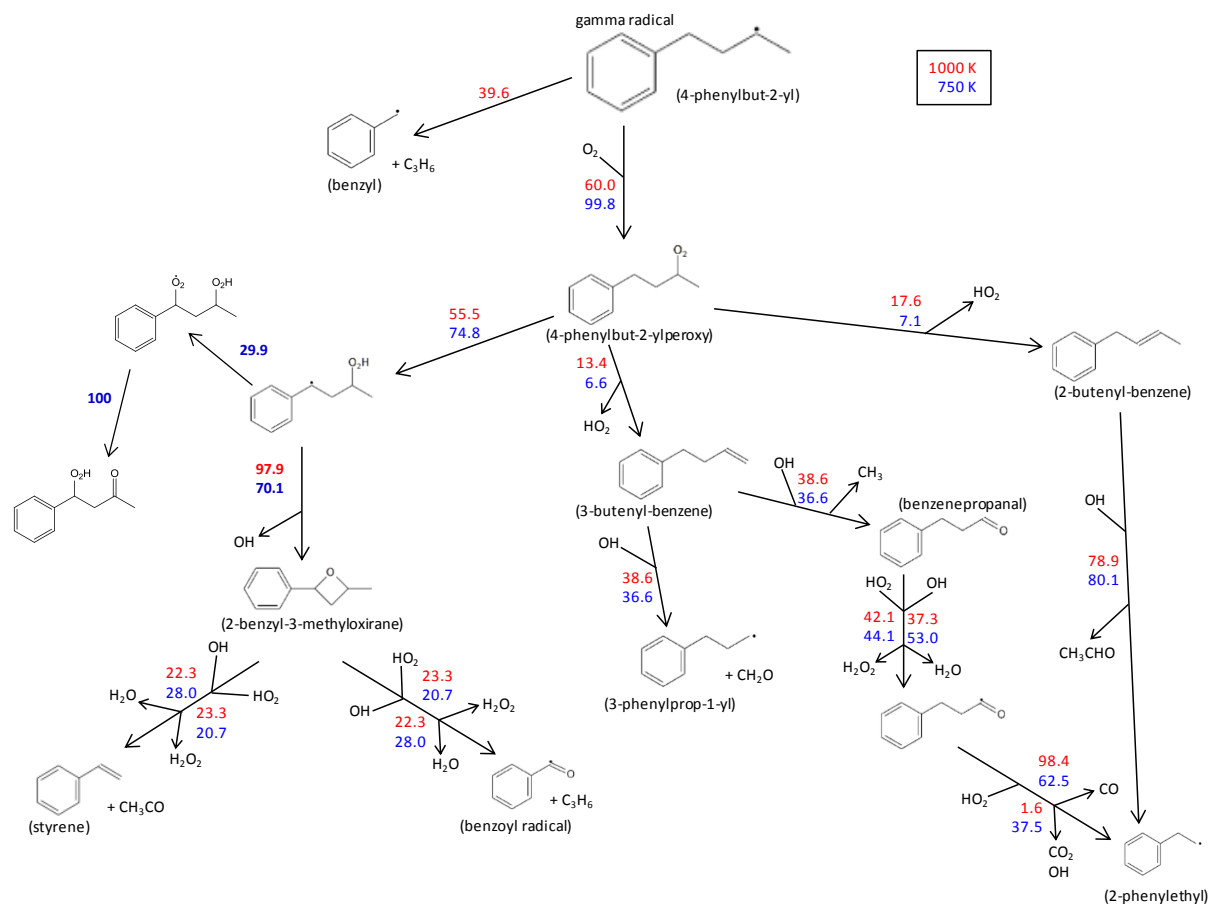


Figure 11: Reaction pathways following gamma (4-phenylbut-2-yl) radical at $\phi = 1.0$, 30 atm and 15 % fuel conversion. Numbers are percent contribution to the consumption of the species on the source side of the arrow.

The remainder reacts with O_2 to form the 4-phenylbut-2-ylperoxy radical. The main consumption pathway of 4-phenylbut-2-ylperoxy radical is via an isomerization reaction to 2-benzyl-3-methyloxirane. However, the importance of the isomerization reaction is lower at 1000 K than at 750 K. Thus, the importance of the other two reactions (2-, and 3-butenyl-benzene formation) are higher at 1000 K compared to those at 750 K.

As shown in Fig. 8, there is no significant difference in the importance of H-atom abstraction reactions at temperatures between 750 K and 1000 K. However, reaction pathways following the H-atom abstraction reactions at 750 K are quite different from those at 1000 K. Typical low-temperature alkyl radical plus molecular oxygen, $\dot{R}+O_2$, and $R\dot{O}_2=QOOH$ isomerization reactions mainly proceed at 750 K, while the fraction of alkyl radical, R, that decomposes to smaller species is very small. As a result, intermediates in the reaction pathways at 750 K are different from those formed at 1000 K.

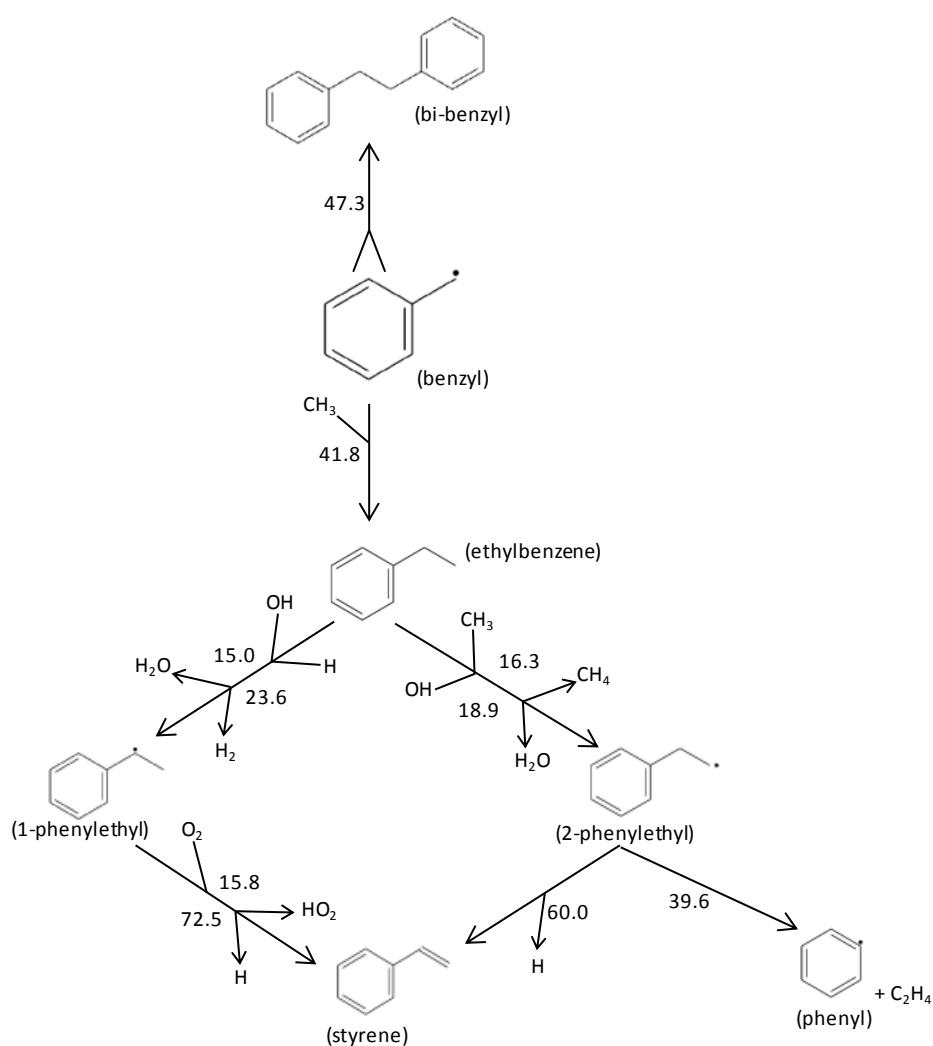


Figure 12: Reaction pathways following unimolecular decomposition of *n*-butylbenzene at 1400K, $\phi = 1.0$, 30 atm and 15% fuel conversion. Numbers are percent contribution to the consumption of the species on the source side of the arrow.

Figure 12 shows reaction pathways following the unimolecular decomposition of the fuel. Since the unimolecular decomposition is significant only at 1400 K, fluxes only at 1400 K are shown. There are two major reaction pathways from the benzyl radical: two benzyl radicals react and bi-benzyl is formed; and benzyl radical reacts with methyl radical to form ethylbenzene. Ethylbenzene undergoes H-atom abstraction reactions to form 1-phenylethyl and 2-phenylethyl radicals. These radicals are subsequently oxidized to styrene. A fraction of 2-phenylethyl radicals decompose to a phenyl radical and ethylene. Therefore, ethylbenzene oxidation plays an important role in the reaction pathway of *n*-butylbenzene subsequent to unimolecular fuel decomposition.

4.5 Sensitivity analysis

A brute force sensitivity analysis including all rate constants was performed using CHEMKIN-Pro at temperatures of 750, 1000 and 1400 K and at a pressure of 30 atm and at an equivalence ratio of 1.0. The analyses were performed by increasing and decreasing both the forward and reverse rate constants by a factor of two, with a sensitivity coefficient expressed using the formula:

$$S = \frac{\ln(\tau_+/\tau_-)}{\ln(k_+/k_-)} = \frac{\ln(\tau_+/\tau_-)}{\ln(2/0.5)}.$$

A positive sensitivity coefficient indicates an inhibiting reaction while a negative sensitivity coefficient indicates a reaction promoting reactivity. Reactions with sensitivity coefficients higher than 0.1 and lower than -0.1 are shown in Fig. 13. We have classified the selected reactions into six groups for explanation: (A) H-atom abstraction reactions on *n*-butylbenzene by $\dot{\text{O}}\text{H}$ radicals; (B) H-atom abstraction by $\text{H}\dot{\text{O}}_2$ radicals on *n*-butylbenzene; (C) fuel decomposition reactions; (D) reactions in the low-temperature oxidation mechanism; (E) reactions of small hydrocarbons and (F) hydrogen-oxygen reactions. The reactions in Group

D are labeled as D1-3 for explanation.

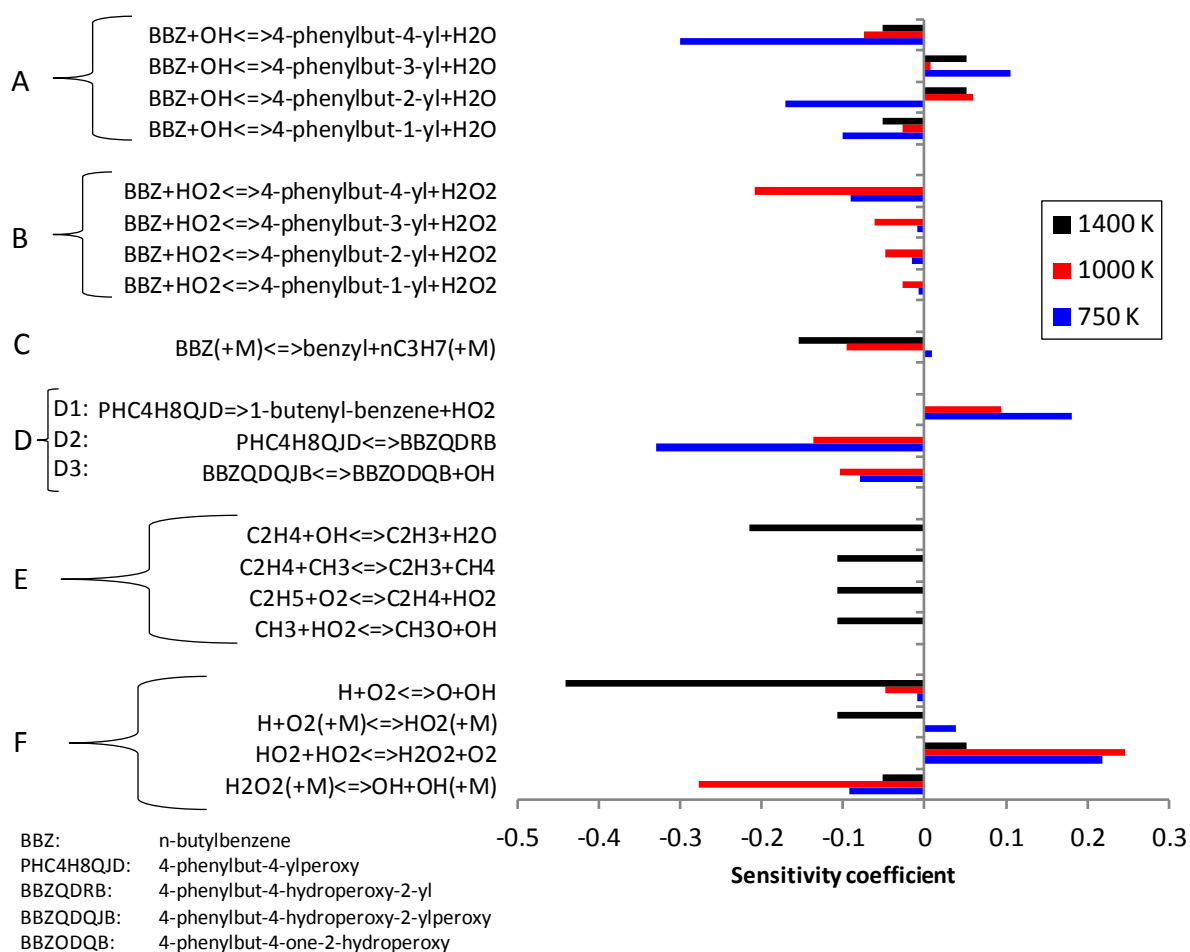


Figure 13: Sensitivity coefficients on ignition delay time of *n*-butylbenzene/air mixture at $\phi = 1.0$ and 30 atm.

For H-atom abstractions by $\dot{\text{O}}\text{H}$ radicals (Group A), the sensitivity coefficients at 750 K are higher than those at 1000 K and 1400 K. On the other hand, for abstraction by $\text{H}\dot{\text{O}}_2$ radicals (Group B), the sensitivity coefficients at 1000 K are higher than those at 750 and 1400 K. The fuel decomposition reactions (Group C), significantly promote reactivity only at 1400 K, with a lesser contribution at 1000 K.

All reactions of Group D can be seen in the low-temperature oxidation process following alpha (4-phenylbut-4-yl) radical (Fig. 9). Alpha radical reacts with molecular oxygen to form 4-phenylbut-4-ylperoxy radical, named PHC₄H₈OJD in Fig. 13. There are competitive

reactions for 4-phenylbut-4-ylperoxy radical consumption: (D1) 1-butenyl-benzene + HO₂ formation reaction and (D2) 4-phenylbut-4-hydroperoxy-2-yl radical (named BBZQDRB in Fig. 13) formation reaction (Path 2 in Fig. 9). At 750 and 1000 K, D1 inhibits reactivity while D2 promotes reactivity. The 1-butenyl-benzene which is produced in D1 reacts with $\dot{\text{O}}\text{H}$ radicals to generate benzaldehyde. On the other hand, 4-phenylbut-4-hydroperoxy-2-yl radical produced in D2 goes to phenyl radical through O₂ addition, $\dot{\text{O}}\text{H}$ radical production and decomposition reactions. In this reaction path (Path 1 in Fig. 9), for each radical entering the reaction chain, three radicals are produced. Path 2 is a chain propagating path leading to HO₂ formation while Path 1 corresponds to the degenerate branching path promoting the low temperature reactivity. As a result, D1 shows a positive sensitivity coefficient while D2 shows a negative one. Moreover, D3 is one of the $\dot{\text{O}}\text{H}$ radical production reactions in Path 2. D3 shows a negative sensitivity with a faster reaction rate of D3 promoting reactivity. D2 and D3 are rate controlling steps in Path 2. Note that D2 and D3 can be classified as $\text{R}\dot{\text{O}}_2 \rightleftharpoons \text{QOOH}$ and $\dot{\text{O}}_2\text{QOOH} \rightleftharpoons \text{carbonylhydroperoxide} + \dot{\text{O}}\text{H}$, respectively.

The reactions of small hydrocarbons (Group E) promote reactivity only at 1400 K. For the hydrogen-oxygen reactions (Group F), the $\dot{\text{O}}\text{H}$ radical formation reaction, $\text{H}_2\text{O}_2(+\text{M}) \rightleftharpoons \dot{\text{O}}\text{H} + \dot{\text{O}}\text{H}(+\text{M})$, through the H₂O₂ formation reactions, $\text{RH} + \text{H}\dot{\text{O}}_2 \rightleftharpoons \dot{\text{R}} + \text{H}_2\text{O}_2$ and $\text{H}\dot{\text{O}}_2 + \text{H}\dot{\text{O}}_2 \rightleftharpoons \text{H}_2\text{O}_2 + \text{O}_2$, significantly affect reactivity at 700 and 1000 K. On the other hand, the chain-branching reaction, $\dot{\text{H}} + \text{O}_2 \rightleftharpoons \ddot{\text{O}} + \dot{\text{O}}\text{H}$, strongly promotes reactivity only at 1400 K.

5. Discussion

n-Butylbenzene exhibits low temperature chemistry and NTC behavior as observed experimentally in the RCM for the higher pressure and equivalence-ratio cases. NTC behavior is also observed for *n*-butylbenzene in other RCM experiments [9] and in jet stirred reactors at

1 atm and 10 atm [22]. However for alkylbenzenes with shorter alkyl chains like *n*-propylbenzene, ethylbenzene and toluene, NTC behavior is not observed in the RCM [9]. Why is NTC behavior present for *n*-butylbenzene, but lacking for the alkylbenzenes with a shorter alkyl chains? Based on our study, we attribute the presence of NTC behavior in *n*-butylbenzene to two reasons. The first reason is the stronger $\dot{R}-O_2$ bond on the alpha site in *n*-butylbenzene (a “secondary” benzylic site) compared to the case of toluene (a “primary” allylic site). The bond strength is about 4 kcal stronger in the *n*-butylbenzene case. Although the $R\dot{O}_2$ adduct for a secondary benzyl radical is much less stable than its alkyl counterpart, this higher activation energy of the decomposition allows for long enough “lifetime” to proceed to further reactions. The second reason is the presence of a facile 6-membered ring isomerization for the alpha- $R\dot{O}_2$ in *n*-butylbenzene but not in *n*-propylbenzene. The extra CH_2 group in *n*-butylbenzene compared to *n*-propylbenzene allows the abstraction of “secondary” H-atoms from the gamma carbon compared to “primary” H-atoms for the gamma carbon in *n*-propylbenzene. The bond strength for a secondary H-atom is about 3 kcal mol^{-1} lower than a primary H-atom leading to a lower activation energy and a faster rate for the associated $R\dot{O}_2$ isomerization in *n*-butylbenzene. This $R\dot{O}_2$ isomerization in *n*-butylbenzene was identified by sensitivity analysis as the reaction (D2) that most promotes ignition at low temperature (750 K, Fig. 13).

The low temperature branching path competes with the concerted elimination of $H\dot{O}_2$. Rate controlling steps for these two paths show up in the sensitivity analysis as the more relevant at 750 K, where the model shows the largest discrepancies with the experiments. Although the reaction rates we included in the mechanism for these reactions are derived from the best available estimations available as of today, high uncertainties are still present. Very limited fundamental studies are available for the oxidation chemistry of secondary allyl radicals and

more extensive investigations extending the results obtained from Altarawneh et al. **Error! Reference source not found.** for ethylbenzene to longer alkyl chain aromatics are needed to constrain the values of the rate constants for the low temperature reaction pathways of these fuels.

6. Comparison with *n*-propylbenzene

Additionally our experimental data has been compared with *n*-butylbenzene data from a supplementary publication by Darcy et al. [44]. This experimental data was carried out to correspond with the data from this paper. *n*-Propylbenzene was studied in both the RCM and shock tube over the temperature range of 650–1600~K at pressures of 1, 10, 30 and 50 and at nominal equivalence ratios of 0.3, 0.5, 1.0 and 2.0. The precise equivalence ratios (Table 2) differ slightly from our *n*-butylbenzene data. Table 2 shows reactant mixture compositions of *n*-propylbenzene used in this study.

Table 2 Composition of mixtures.

ϕ	% fuel	% O ₂	% diluent
0.29	0.50	20.89	78.61
0.48	0.83	20.83	78.34
0.96	1.65	20.65	77.70
1.92	3.25	20.32	76.43

Figures 14–16 show comparisons of the *n*-propylbenzene and the *n*-butylbenzene experimental data at the four nominal equivalence ratios and at 10, 30 and 50 atm. Experiments at 1 atm reflected shock pressure were only possible in the shock tube and not in the RCM. They have been discussed in detail in a previous publication [44]. In the comparisons, *n*-propylbenzene is represented by black symbols (solid symbols: ST, open symbols: RCM) and lines (solid line: adiabatic simulation, dashed line: facility effect simulation) while *n*-butylbenzene is represented by red symbols and lines.

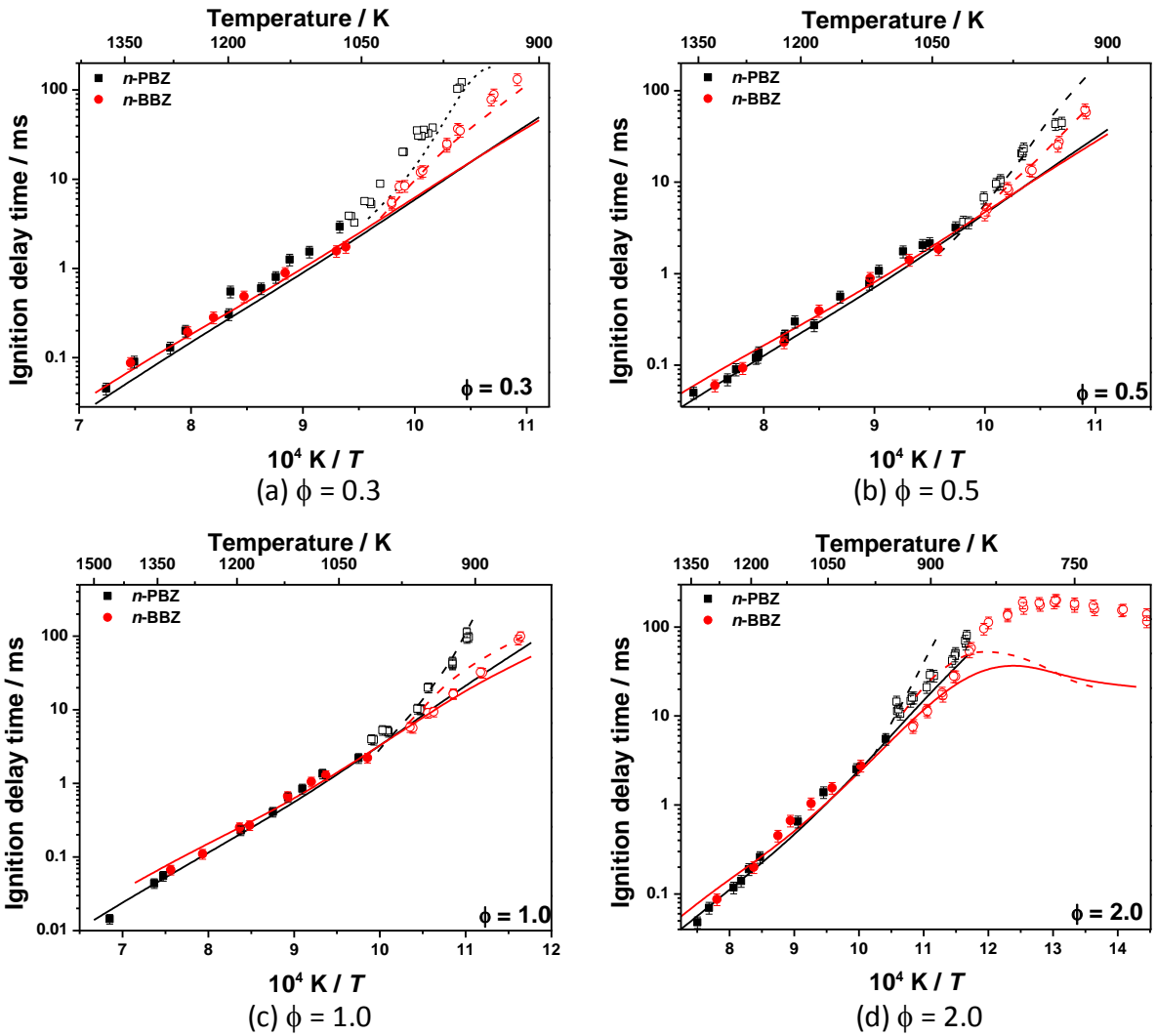


Figure 14: A comparison of *n*-propylbenzene and *n*-butylbenzene at various equivalence ratios (ϕ) and at 10 atm. ■ *n*-propylbenzene data, ● *n*-butylbenzene data. Solid symbols: Shock tube, Open symbols: RCM. Simulation; --- RCM simulations including facility effects, — adiabatic simulations.

At a pressure of 10 atm, Figs. 14(a)–14(d), it is clear that *n*-propylbenzene and *n*-butylbenzene experience similar high-temperature chemistry as both the experimental data and the mechanism predictions show nearly the same ignition delay times above 1100 K.

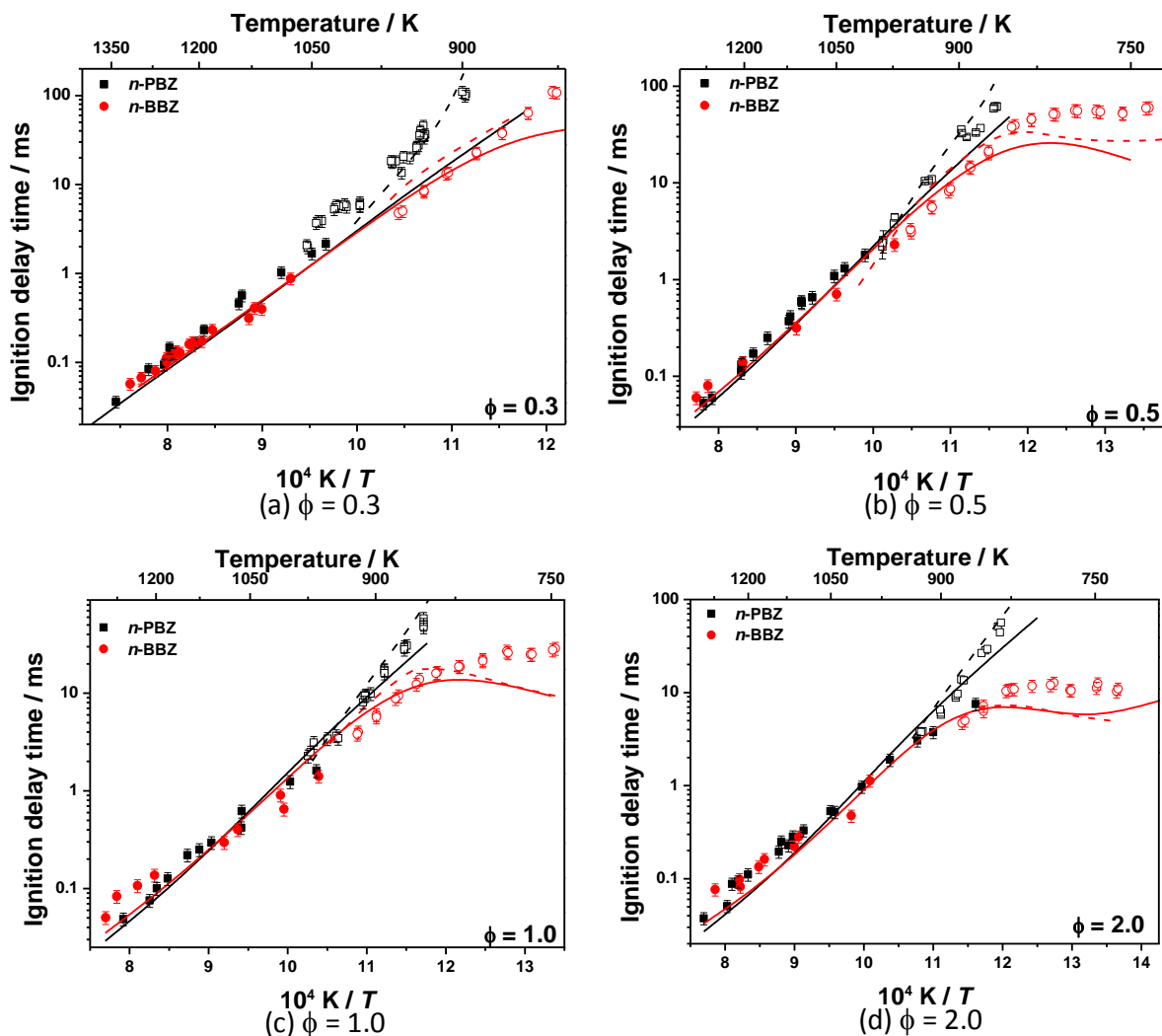
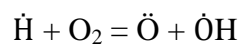


Figure 15: A comparison of *n*-propylbenzene and *n*-butylbenzene at various equivalence ratios (ϕ) and at 30 atm. \blacksquare *n*-propylbenzene data, \bullet *n*-butylbenzene data. Solid symbols: Shock tube, Open symbols: RCM. Simulation; --- RCM simulations including facility effects, — adiabatic simulations.

At lower temperatures the reactivity of *n*-butylbenzene becomes stronger which results in faster ignition delay times observed in both experiments and model predictions. The longer alkyl side chain of *n*-butylbenzene is important at low and intermediate temperatures, which allows more facile intra-molecular hydrogen atom isomerization reactions in the case of *n*-butylbenzene compared to *n*-propylbenzene. It is interesting to note is that only at fuel-rich conditions do we observe any negative temperature coefficient behavior for *n*-butylbenzene and it is not observed at all for *n*-propylbenzene, Fig. 14(d).

Similar trends are observed at 30 atm pressure Figs. 15(a)–15(d) in which *n*-propylbenzene shows longer ignition delay times at lower temperatures while at higher temperatures there is a convergence of the data where it seems to have almost identical reactivity. This is understandable as the main chain branching at higher temperatures is:



which is dependent upon the concentration of molecular oxygen which is maintained constant in the reactant mixtures for each fuel. As the O₂ concentration is quite similar in both mixtures the high temperature reactivity is quite similar. Once again at lower temperatures, the alkyl group determines the fuel's reactivity and, while both fuel mixtures have similar compositions at the varying equivalence ratios, *n*-butylbenzene has a longer (C4) alkyl side chain compared to *n*-propylbenzene (C3). Low temperature chemistry is dominated by chain branching and chain propagation reactions and internal hydrogen atom isomerization reactions involving 5-, 6-, 7-, and 8-membered transition state ring structures. These are more facile as the alkyl side-chain length becomes longer.

At 50 atm reflected shock pressures, Fig. 16, similar trends are observed to those which have already been discussed in which as the temperature decreases *n*-butylbenzene shows higher reactivity as opposed to *n*-propylbenzene. Once again NTC-like behavior is observed for *n*-butylbenzene while it is not prevalent for *n*-propylbenzene conditions.

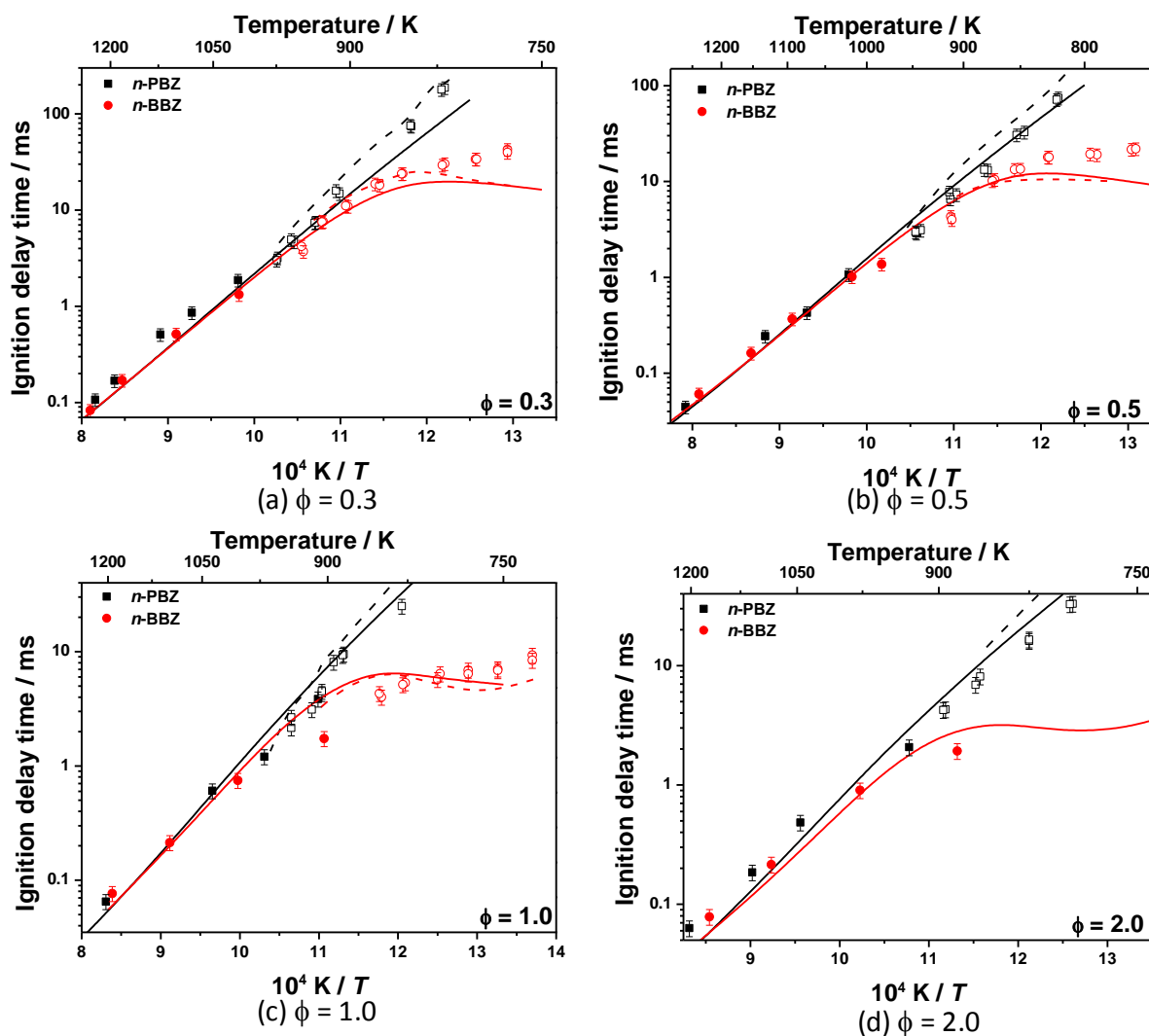


Figure 16: A comparison of *n*-propylbenzene and *n*-butylbenzene at various equivalence ratios (ϕ) and at 50 atm. ■ *n*-propylbenzene data, ● *n*-butylbenzene data. Solid symbols: Shock tube, Open symbols: RCM. — Simulation; --- RCM simulations including facility effects, — adiabatic simulations.

6. Conclusions

A comprehensive study of *n*-butylbenzene oxidation in air was carried out using a rapid compression machine and shock tube over a wide range of temperature (730–1360 K), pressure (1, 10, 30 and 50 atm) and equivalence ratio (0.3, 0.5, 1.0 and 2.0). The chemical kinetic model validated with shock tube data was modified by adding low-temperature chemical kinetics and the predictions with the modified model were in good agreement with the measured ignition delay times over this wide range of temperature, pressure and

equivalence ratio conditions. Some discrepancies between model calculations and experiments were observed in the low temperature region. The detailed and complicated process of *n*-butylbenzene oxidation was examined via reaction flux analysis and important reactions were identified by both analyses. In the high-temperature region, the fuel decomposition reaction and $\dot{\text{H}} + \text{O}_2 = \ddot{\text{O}} + \dot{\text{O}}\text{H}$ dominated the sensitivity and reactions of small hydrocarbons showed higher sensitivity to ignition delay times. In the low-temperature region (600–1000 K), predicted ignition delay times showed high sensitivity to the low-temperature oxidation pathways, particularly to the alpha (4-phenylbut-4-yl) radical, and subsequent $\text{R}\dot{\text{O}}_2 \rightleftharpoons \text{QOOH}$ and $\dot{\text{O}}_2\text{QOOH} \rightleftharpoons \text{carbonylhydroperoxide} + \dot{\text{O}}\text{H}$ reactions. These results highlight the need for a more extensive fundamental investigation of the low temperature oxidation paths of alkyl aromatic structures with particular emphasis on the secondary benzyl + O₂ system.

A comparison was made between *n*-propylbenzene and *n*-butylbenzene data obtained over the same range of conditions. A consistent trend was observed throughout the data in which the reactivity of both fuels is very similar while at high temperatures but *n*-butylbenzene was shows higher reactivity than *n*-propylbenzene at lower temperatures. This difference at low temperature was attributed to the wider variety of low temperature reactions available to the *n*-butyl compared to the *n*-propyl side-chain.

Acknowledgements

NUIG acknowledge the financial support of the Saudi Arabian Oil Company. The LLNL work was performed under the auspices of the US Department of Energy by Lawrence Livermore National Laboratory under Contract DE-AC52-07NA27344 and was supported by the US Department of Energy, Office of Vehicle Technologies (program manager Gurpreet Singh). Co-author HN acknowledges the financial support "Young Researcher Overseas Visits Program for Vitalizing Brain Circulation" from Japan Society of the Promotion for Science.

References

- [1] F. Battin-Leclerc, *Prog. Energy Combust. Sci.* 34(4) (2008) 440–498.
- [2] J. T. Farrell, N. P. Cernansky, F. L. Dryer, D. G. Friend, C. A. Hergart, C. K. Law, R. McDavid, C. J. Mueller, H. Pitsch, Society of Automotive Engineers, SAE Paper 2007-01-0201 (2007).
- [3] C. J. Mueller, W. J. Cannella, T. J. Bruno, B. Bunting, H. D. Dettman, J. A. Franz, M. L. Huber, M. Natarajan, W. J. Pitz, M. A. Ratcliff, K. Wright, *Energy Fuels* 26(6) (2012) 3284–3303.
- [4] D. F. Davidson, B. M. Gauthier, R. K. Hanson, *Proc. Combust. Inst.* 30 (2005) 1175–1182.
- [5] R. Sivaramakrishnan, R. S. Tranter, K. Brezinsky, *Proc. Combust. Inst.* 30 (2005) 1165–1173.
- [6] G. Mittal, C.-J. Sung, *Combust. Flame* 150(4) (2007) 355–368.
- [7] R. P. Lindstedt, L. Q. Maurice, *Combust. Sci. Technol.* 120(1-6) (1996) 119–167.
- [8] Y. Sakai, A. Miyoshi, M. Koshi, W. J. Pitz, *Proc. Combust. Inst.* 32 (2009) 411–418.
- [9] A. Roubaud, R. Minetti, and L.R. Sochet, *Combust. Flame* 121(3) (2000) 535–541.
- [10] K. Brezinsky, *Prog. Energy Combust. Sci.* 12(1) (1986) 1–24.
- [11] C. Ellis, M.S. Scott, R.W. Walker, *Combust. Flame* 132 (2003) 291–304.
- [12] K. Narayanaswamy, G. Blanquart, H. Pitsch, *Combust. Flame* 157(10) (2010) 1879–1898.
- [13] M. K. Altarawneh, B. Z. Dlugogorski, E. M. Kennedy, J. C. Mackie, *Combust. Flame* 160(1) (2013) 9–16.
- [14] H.-P. S. Shen, M. A. Oehlschlaeger, *Combust. Flame* 156(5) (2009) 1053–1062.
- [15] A. Roubaud, O. Lemaire, R. Minetti, L. R. Sochet, *Combust. Flame* 123(4) (2000) 561–571.
- [16] F. Battin-Leclerc, R. Bounaceur, N. Belmekki, P-A. Glaude, *Int. J. Chem. Kinet.* 38(4)

- (2006) 284–302.
- [17] S. Gudiyella, T. Malewicki, A. Comandini, K. Brezinsky, *Combust. Flame* 158(4) (2011) 687–704.
- [18] S. Gaïl, P. Dagaut, *Combust. Flame* 141(3) (2005) 281–297.
- [19] S. Gudiyella, K. Brezinsky, *Combust. Flame* 159(3) (2012) 940–958.
- [20] D. Darcy, C. J. Tobin, K. Yasunaga, J. M. Simmie, J. Würmel, W. K. Metcalfe, T. Niass, S. S. Ahmed, C. K. Westbrook, H. J. Curran, *Combust. Flame* 159 (2012) 2219–2232.
- [21] M. Ribaucour, A. Roubaud, R. Minetti, L. R. Sochet, *Proc. Combust. Inst.* 28 (2000) 1701–1707.
- [22] B. Husson, R. Bounaceur, K. Tanaka, M. Ferrari, O. Herbinet, P.-A. Glaude, R. Fournet, F. Battin-Leclerc, M. Crochet, G. Vanhove, R. Minetti, C. J. Tobin, K. Yasunaga, J. M. Simmie, H. J. Curran, T. Niass, O. Mathieu, S. S. Ahmed, *Combust. Flame* 159 (2012) 1399–1416.
- [23] P. Diévert, P. Dagaut, *Proc. Combust. Inst.* 33 (2011) 209–216.
- [24] S. H. Won, S. Dooley, F. L. Dryer, Y. Ju, *Combust. Flame* 159 (2012) 541–551.
- [25] C. Ji, E. Dames, H. Wang, F. N. Egolfopoulos, *Combust. Flame* 159 (2012) 1070–1081.
- [26] E. Pousse, P.-A. Glaude, R. Fournet, F. Battin-Leclerc, *Combust. Flame* 156 (2009) 954–974.
- [27] W. S. Affleck, A. Thomas, *Proc. Inst. Mech. Eng.* 183 (1968) 365–385.
- [28] L. Brett PhD Thesis 1999, National University of Ireland, Galway.
- [29] L. Brett, J. MacNamara, P. Musch, J. M. Simmie, *Combust. Flame* 124 (2001) 326–329.
- [30] J. Würmel, J. M. Simmie, H. J. Curran, *Int. J. Vehicle Design* 44 (2007) 84–106.
- [31] P. Beeley, P. Gray, J. F. Griffiths, *Proc. Combust. Inst.* 17 (1979) 1415–1423.
- [32] G. Mittal, C.-J. Sung, *Combust. Sci. Technol.* 179(3) (2007) 497–530.
- [33] C. Morley, *Gaseq, Version 0.76*, <http://www.gaseq.co.uk> (2004).

- [34] S. M. Gallagher, H. J. Curran, W. K. Metcalfe, D. Healy, J. M. Simmie, G. Bourque, *Combust. Flame* 153 (2008) 316–333.
- [35] D. Healy, N. S. Donato, C. J. Aul, E. L. Petersen, C. M. Zinner, G. Bourque, H. J. Curran, *Combust. Flame* 157 (2010) 1526–1539.
- [36] W. M. Haynes, *CRC Handbook of Chemistry and Physics*, CRC Press, 91st Edition, 2010 6–110.
- [37] D. Darcy, PhD Thesis 2013, National University of Ireland, Galway.
- [38] R. Mével, P. A. Boettcher, J. E. Shepherd, *Chem. Phys. Lett.* 531 (2012) 22–27.
- [39] W. K. Metcalfe, S. M. Burke, S. S. Ahmed, H. J. Curran, “A Hierarchical and Comparative Kinetic Modeling Study of C₁–C₂ Hydrocarbon and Oxygenated Fuels”, *Int. J. Chem. Kinet.* (2013) accepted DOI: 10.1002/kin.20802.
- [40] W. K. Metcalfe, S. Dooley, F. L. Dryer, *Energy Fuels* 25(11) 4915–4936 (2011).
- [41] D. Darcy, M. Mehl, J. M. Simmie, J. Würmel, W. K. Metcalfe, C. K. Westbrook, W. J. Pitz, H. J. Curran, *Proc. Combust. Inst.* 34 (2013) 411–418.
- [42] C. Cavallotti, D. Polino, A. Frassoldati, E. Ranzi, *J. Phys. Chem. A* 116 (2012) 3313–3324.
- [43] R. G. Butler, I. Glassman, *Proc. Combust. Inst.* 32 (2009) 395–402.
- [44] D. Darcy, H. Nakamura, C. J. Tobin, M. Mehl, W. K. Metcalfe, W. J. Pitz, C.K. Westbrook, H. J. Curran, “A High-Pressure Rapid Compression Machine Study of *n*-Propylbenzene Ignition”, *Combust. Flame* (2013) submitted.
- [45] M. Mehl, W. J. Pitz, C. K. Westbrook, K. Yasunaga, C. Conroy, H. J. Curran, *Proc. Comb. Inst.* 33 (2011) 201–208.
- [46] Y. Murakami, T. Oguchi, K. Hashimoto, Y. Nosaka, *J. Phys. Chem. A* 113 (2009) 10652–10666.
- [47] M. Altarawneh, B. Z. Dlugogorski, E.M. Kennedy, J. C. Mackie, *Proc. Combust. Inst.*

34 (2013) 315–323.

[48] E. R. Ritter, J. W. Bozzelli, *Int. J. Chem. Kinet.* 23 (1991) 767–778.

[49] T. H. Lay, J. W. Bozzelli, A.M. Dean, E.R. Ritter, *J. Phys. Chem.* 99 (1995) 14514–14527.

[50] R. Minetti, M. Ribaucour, M. Carlier, C. Fittschen, L. R. Sochet, *Combust. Flame* 96 (1994) 201–211.